

Depth, bed slope and wave climate dependence of long term average sand transport across the lower shoreface

D.C. Patterson*, P. Nielsen

School of Civil Engineering, University of Queensland, Australia

ARTICLE INFO

Article history:

Received 10 February 2016
Received in revised form 24 May 2016
Accepted 23 July 2016
Available online 10 August 2016

Keywords:

Cross-shore sand transport
Equilibrium
Profile evolution
Shoreface
Bed slope

ABSTRACT

We analyse measured 46 year changes in nearshore bathymetry to quantify rates of net shore-normal sand transport (q_x) in 10–20 m depths at northern Gold Coast, Australia. These are significant both in understanding local disequilibrium shoreface evolution and as prototype data that may be used to assess theoretical predictive methods. This analysis is feasible because the migration history of a nearby river mouth has formed a disequilibrium shoreface lobe that is evolving towards an equilibrium profile shape, which is identified in adjacent non-lobe profiles. The data include various profile transect surveys from 1966 to 2012, sediment characteristics and locally recorded wave conditions.

A generally applicable form of q_x that is a function of both a depth-dependent horizontal bed transport forcing component and bed slope $q_x = q_x(h, S)$ is developed and quantified in terms of long term average behavior for this site. Dependence of the forcing component on wave climate is shown from higher than average q_x derived from the lobe response during a recent five year period with abnormally high waves. Our $q_x(h, S)$ quantifies the balance between generally shoreward wave boundary layer sand transport and the opposing effect of the seabed slope, as incorporated in the predictive methods.

© 2016 Elsevier B.V. All rights reserved.

1. Introduction

The ability to predict sand transport under non-breaking waves across the lower shoreface is important for understanding the rate of recovery of beaches after major storm erosion, the behavior of nourishment sand placed there and shoreface profile evolution with changing sea level. Various predictive relationships have been developed (Bailard, 1981; Nielsen, 1992, 2006; Nielsen and Callaghan, 2003; Van Rijn et al., 2004) but there is a general lack of suitable prototype data for assessment and verification of those methods. They are not proven under accreting conditions, either in the laboratory with fixed wave height (H) and period (T) or in the field with H , T varying over years. The present study provides a calibration opportunity for this longer time scale. We investigate the shoreface profile shape, evolution and shore-normal sediment transport from comprehensive transect surveys over the 46 years 1966–2012 at northern Gold Coast, Australia (Fig. 1).

2. Study site coastal processes

2.1. Coastal morphology

The study site lies within a large coastal unit extending from the Clarence River to Moreton Island (Fig. 1 left) with a series of long

embayed sand beaches controlled in location and alignment by bedrock headlands, along which there is a continuous northward wave-induced flow of sand within the littoral zone. The entire active coastal and river mouth system consists of Holocene deposits of fine, well-sorted and rounded quartzose marine sand of 0.22 mm median grain size. The local study site (Fig. 1 right) lies within the Gold Coast beach embayment where the shoreface extends from the beach to about 20–25 m depth, beyond which the profile transitions to the 30 km wide continental shelf.

2.2. Incident waves

Wave conditions have been recorded using Waverider buoys since 1986 at a location in about 17 m water depth immediately offshore from the site (Fig. 1), including directional data since 2007. Long term local significant wave height (H_s) and spectral peak period (T_p) statistics are shown in Fig. 2, indicating a median H_s of about 1.05 m and T_p most commonly in the range 7–12 s. Wave directions lie predominantly in the range 70 to 125 degrees, with east-southeast sector dominance.

2.3. Regional alongshore sand transport regime

Alongshore sand transport and the beach system sediment budget of the Gold Coast have been extensively monitored and investigated for

* Corresponding author.
E-mail address: deamari@powerup.com.au (D.C. Patterson).

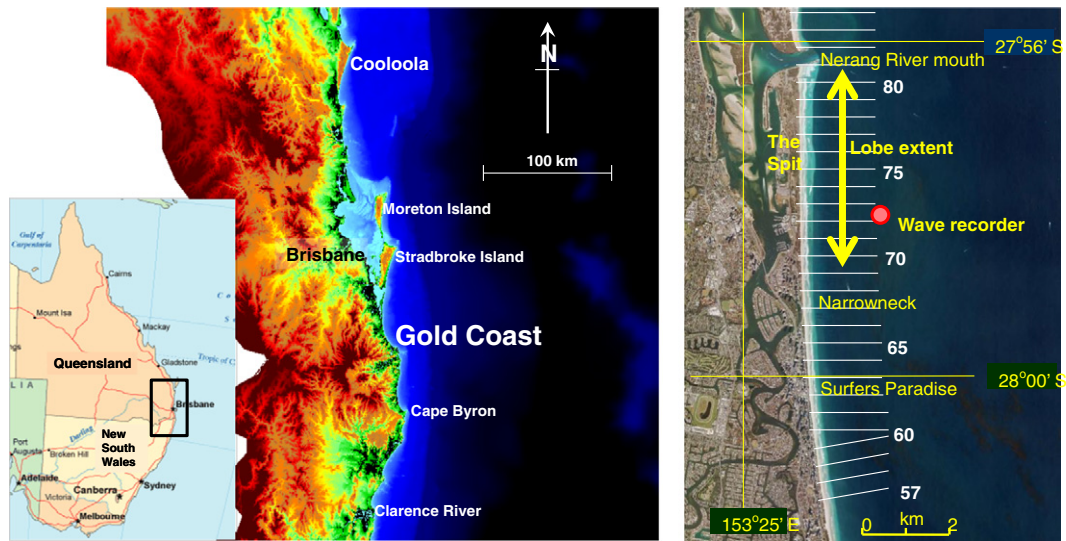


Fig. 1. Australia's Gold Coast location (left) and location of lobe and survey transects (right).

>50 years. The alongshore sand transport regime has been calculated from wave data recorded regionally in deep water (80 m) and validated by correlation with sand bypassing at river mouths and adjacent sand volume changes at both the southern and northern ends of the Gold Coast beach system. It is established that there is an annual average net northward sand transport from the south of about 550,000 m³/yr. Two-dimensional modelling (Patterson, 1999; Andrews and Nielsen, 2001) shows that this alongshore transport is driven by wave-induced surf zone radiation stresses, predominantly at <5 m depth and negligible at >10 m. Here, we refer to that zone as the 'littoral zone'.

The sand bypassing rate at the Nerang River entrance needed to keep pace with the sand supply and maintain the adjacent shoreline averages

about 630,000 m³/yr, indicating a higher net rate of alongshore transport there than is supplied further south. Patterson (2007a,b) used recorded deep water wave data and bathymetry surveys to show that this increase occurred between Narrow Neck and the river entrance and that the positive gradient was compensated by a net supply from the lower shoreface into the littoral zone of about 80,000 m³/yr along that 5 km part of the coast.

2.4. Nerang River mouth migration history

The coastal dune topography indicates that the Nerang River entrance has undergone repeated cycles of alongshore migration along the area north from Narrowneck (Fig. 3) to at least its present location

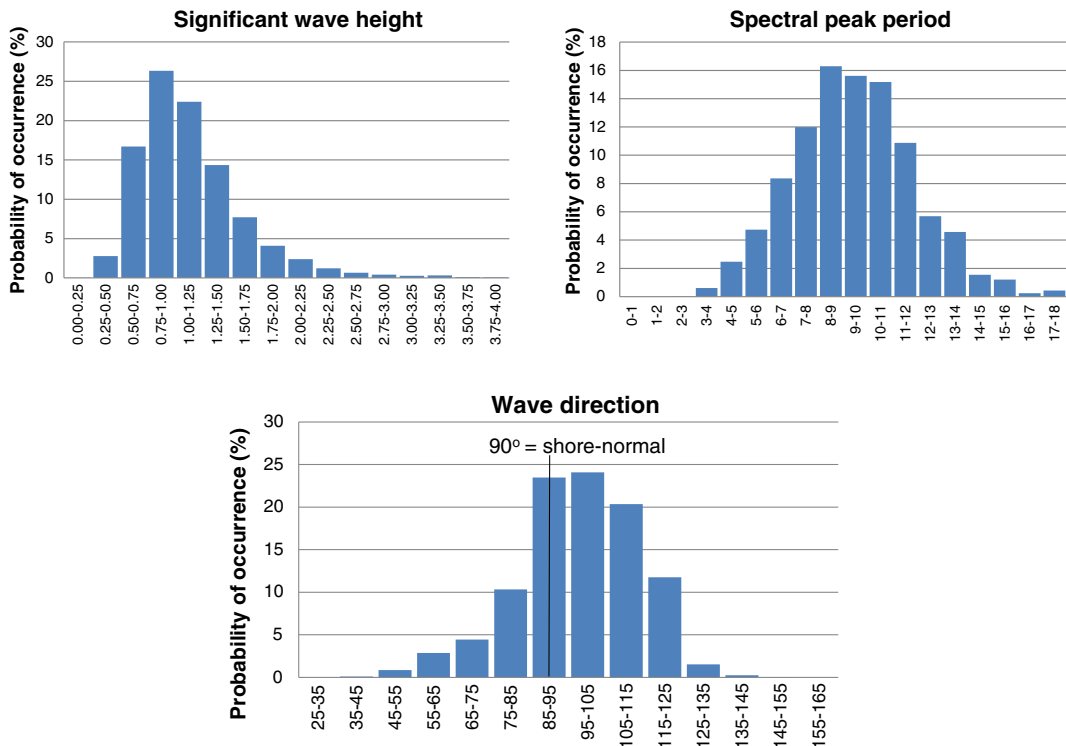


Fig. 2. Wave height, period and direction occurrences at Gold Coast wave recorder.

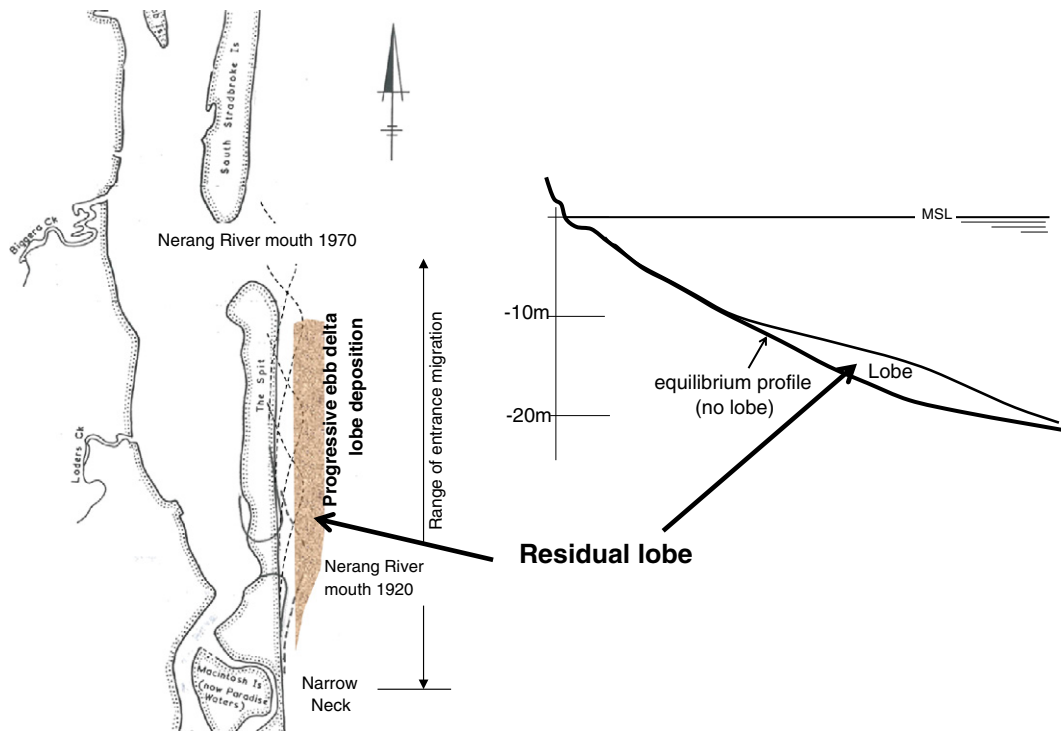


Fig. 3. Recent historical migration of the Nerang River mouth.

over centuries to millennia. The recent history of movement of the entrance from about 1920 is shown in Fig. 3. The river mouth was stabilised by training wall construction and sand bypassing in 1986 (Fig. 1).

2.5. Shoreface profile morphology and dynamics

Transect surveys (Fig. 1) undertaken regularly since 1966 extend from the dune to water depths generally of 20–25 m. The local tidal range is approximately 1 m. Repetitive surveys show how the profiles respond cyclically to cyclone events with $H_s > 5-6$ m to about water depth (h) = 10–13 m (Fig. 4). While these processes may involve large exchanges of sand, erosion and accretion volumes associated with storm events are typically in balance, with dynamic stability over

the longer term. Hallermeier (1977) suggests a limiting depth of profile change = $2.28H(1-4.78H/L_o)$, where H is the significant wave height exceeded for 12 h per year, giving a depth of 9–10 m for the recorded Gold Coast data, consistent also with the seaward limit of the along-shore littoral transport zone (h_{LT}). That formulation yields 11–12 m for the more extreme prevailing cyclone conditions $H_s = 6$ m and $T_p = 11$ s, consistent with that shown in Fig. 4. The shoreface profile shape below h_{LT} exhibits little or no bed level change over time.

Hallermeier (1981) further suggests a limiting depth (h_i) of significant net cross-shore sand transport, which corresponds to the depth from which any long term (centuries to millennia) supply of sand from the inner shelf to the coastal system is feasible, given as $H_{sm}T_{sm}(g/5000d_{50})^{0.5}$, where subscript m denotes the long term median values and T_s is the significant wave period. The recorded Gold Coast

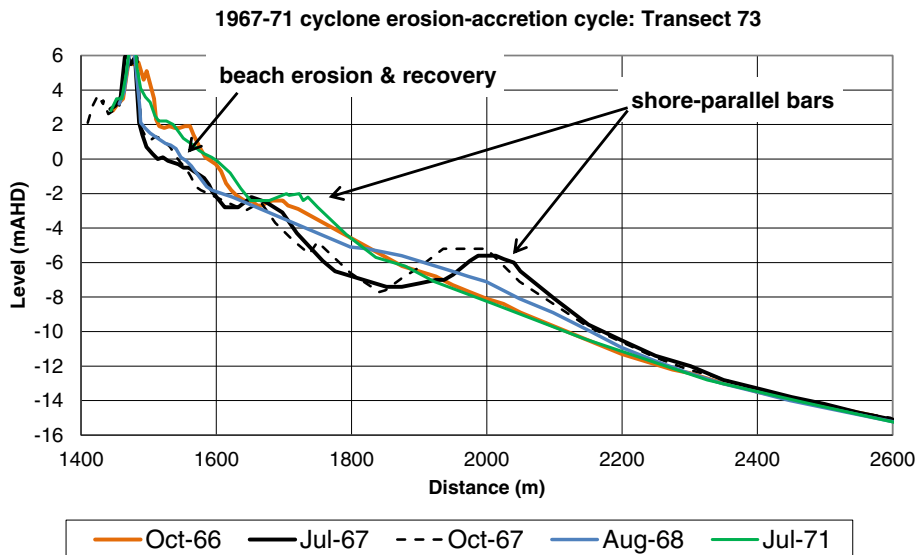


Fig. 4. Erosion and accretion cycle associated with the major cyclone event in June 1967.

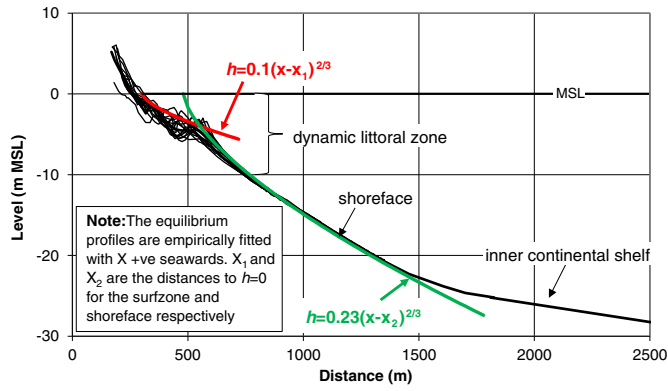


Fig. 5. Typical northern Gold Coast non-lobe profile (Transect 63).

wave data indicates $H_{sm} = 1.05$ m and $T_{sm} = 8.4$ s, yielding a limiting depth (h_i) of about 26 m. This is very close to the transition from the steeper shore-face to the flatter inner continental shelf (Fig. 5).

2.6. Identification of disequilibrium lobe

The existence of coastal equilibrium profiles that maintain their long term average shape has been recognized for many years (Bruun, 1954, 1962, 1986; Dean, 1977, 1991). Bruun (1954) and Dean (1977) analysed extensive data sets from the Danish West coast, California and along the Atlantic and Gulf coasts of United States found that a power law of general form $h = Ax^n$ with $n = 2/3$ provided the best overall fit to the measured profile shapes. Inman et al. (1993) and Larson et al. (1999) divided the profile into two portions that correspond to the regions with breaking and non-breaking waves respectively on the basis that the region where wave breaking prevails may be treated separately from the offshore zone where mainly non-breaking waves control the profile shape.

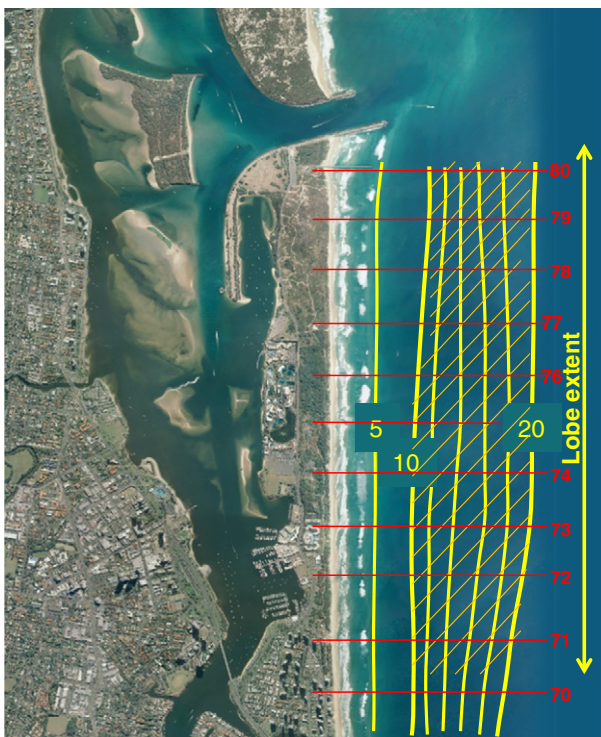


Fig. 6. Shoreface lobe bathymetry showing alongshore uniformity north of Transect 72.

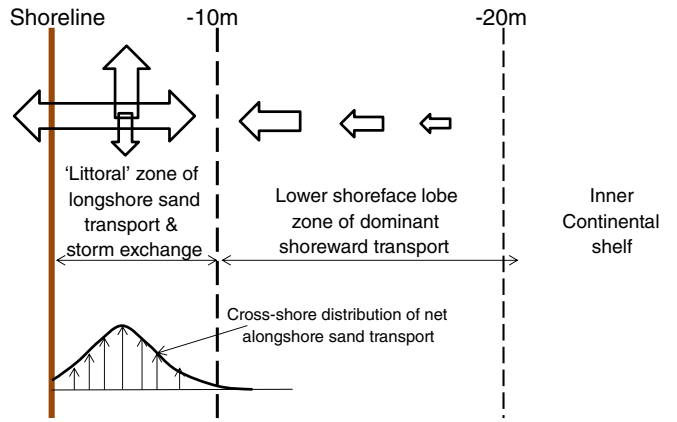


Fig. 7. Conceptual model of lower shoreface lobe sand supply to littoral zone.

At the Gold Coast, the dynamically active surf zone area may be matched empirically to the $h = Ax^{2/3}$ profile, with $A \approx 0.1 \text{ m}^{1/3}$. However that shape does not match that across the lower shoreface zone of non-breaking waves (Fig. 5). Along the coastline south of about Transect 65, the lower shoreface profiles are all consistent and unchanging, indicating the long term average shape which, despite a lack of theoretical basis, may also be matched approximately to $h = Ax^{2/3}$, where in that case $A \approx 0.23 \text{ m}^{1/3}$. In deeper water, that shape deviates from the measured shape where the profile transitions to the inner continental shelf through the depth range 22–25 m (Fig. 5).

A notable exception to this lower shoreface ‘equilibrium’ profile shape occurs along the Spit (Fig. 1). There, sand has deposited in the lower shoreface and created a ‘lobe’ that is the residual lower part of former Nerang River ebb delta abandoned as the river mouth migrated northward. The lobe is still evident in the profiles as far as 5 km south of the present entrance location, north from about Transect 68. The lobe bathymetry is shown in Fig. 6 as depth contours, illustrating its alongshore uniformity at depths $h > 10\text{--}12$ m north from Transect 72 and a transition to the non-lobe area to the south.

3. Conceptual model of shoreface sand supply

3.1. Shoreface versus littoral zone processes

The conceptual distinction between the lower shoreface and the littoral zone of wave induced alongshore transport and cross-shore exchanges of sand associated with storm erosion is illustrated in Fig. 7. This shows the net shoreward supply of sand from the disequilibrium lobe area into the littoral system as a key contributor to the beach sand budget.

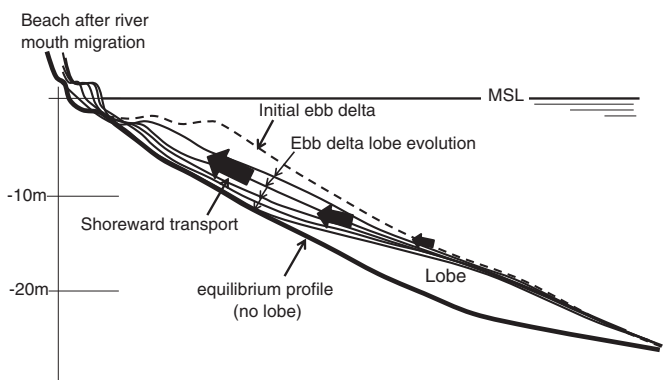


Fig. 8. Conceptual long term evolution of ebb delta lobe.

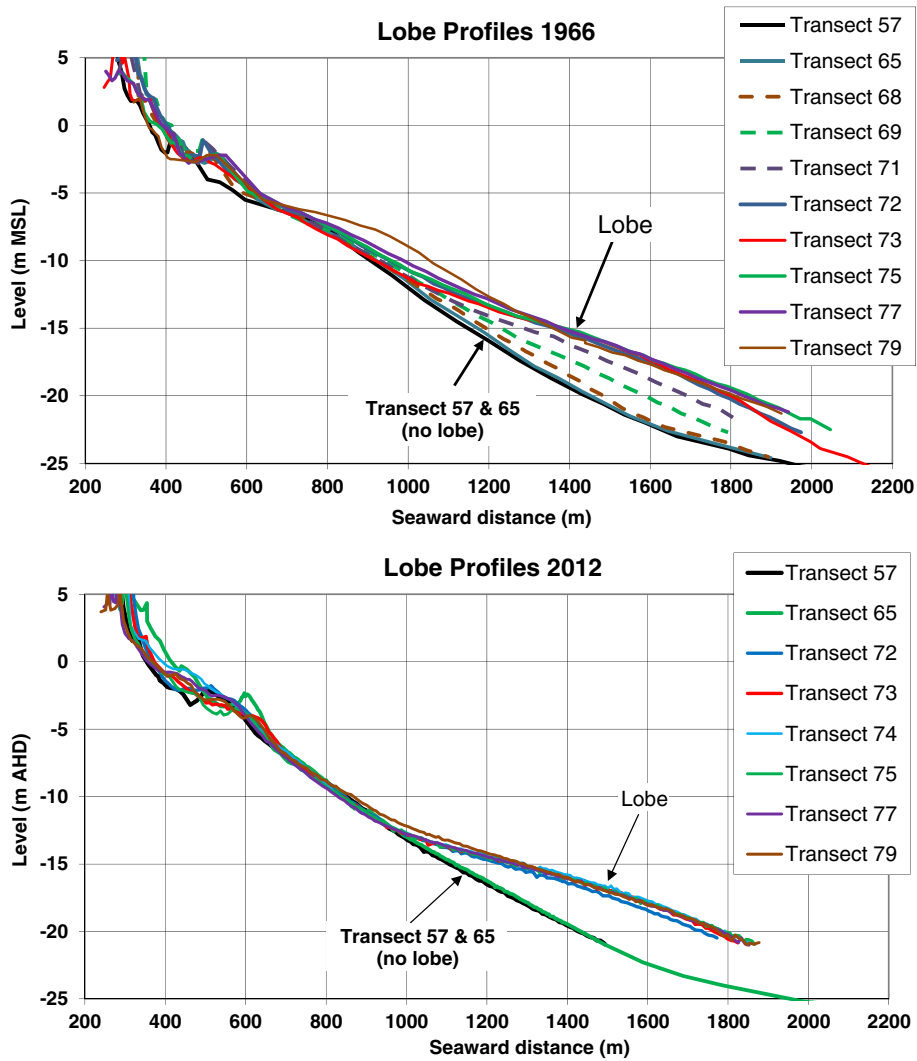


Fig. 9. Simultaneous lobe profiles in 1966 (top) and 2012 (bottom) showing extensive evolution towards the equilibrium shape.

3.2. Analysis of sand transport

For this study, we examine both the equilibrium profile shape and the long term morphological evolution of the non-equilibrium

lobe. Particularly, the surveys show that the lobe bathymetry is relatively uniform along its 4 km extent and is evolving progressively towards the equilibrium shape. We have analysed the cumulative bed level changes to derive long term average rates of shoreward

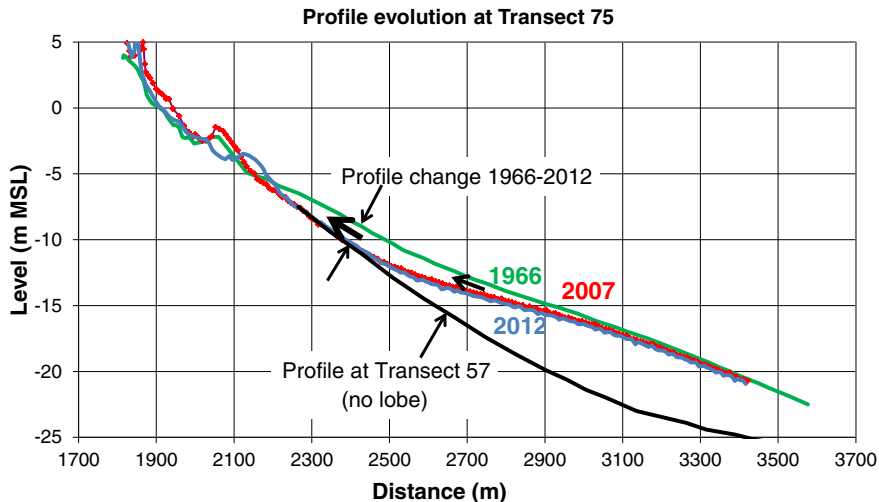


Fig. 10. Lobe profile depletion towards equilibrium at Transect 75 - 1966–2012.

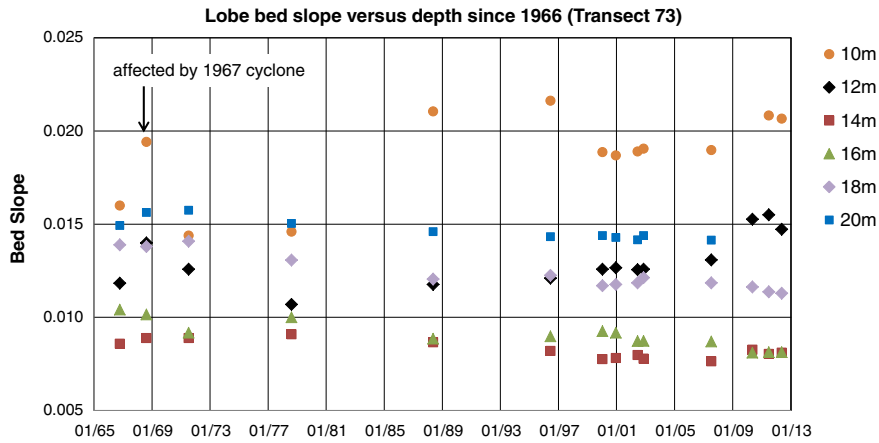


Fig. 11. Change in seabed slope (S) at various depths (h_i) at Transect 73 since 1966.

sand transport from the mid to lower shoreface, as shown conceptually in Fig. 8.

In this paper, we describe the lower shoreface profile dynamics, from which we identify the non-lobe equilibrium profile shape and the nature and evolution of the disequilibrium lobe. Lobe bed level and bed slope (S) changes through time yield average shore-normal sand transport rates $q_x(h,S)$ between the dates of survey analysed, from which a general form of depth and bed slope dependency is derived in terms of a depth dependent equivalent horizontal bed component $q_x(h,0)$ and a slope factor. The effect of wave climate on q_x is investigated by comparing a shorter 5 year period with unusually high waves with the 46 year longer term average rates. Results obtained from the predictive method of van Rijn et al. (2004) for a horizontal bed (without bed slope adjustment) for the 5 year period for which comprehensive wave data are available are compared with the equivalent measured $q_x(h,0)$ rates.

4. Shoreface lobe evolution

The lobe is now a residual feature, isolated from and behaving independent of the processes at the present river entrance in response to the incident wave climate. The lobe in 1966 was interpreted by Patterson (2007a, 2013) from the ‘bulge’ shape of the profiles at depths $8-10\text{ m} < h < 25\text{ m}$ that are markedly different from the ‘equilibrium’ shape further south, for example at Transects 57 and 65 (Fig. 9 top). The subsequent surveys show that the disequilibrium lobe profiles have been depleted of sand progressively over time in a characteristic

manner, most markedly in the shallower parts and decreasing with depth. This has modified the profiles in a manner that is trending towards the equilibrium shape.

In 1966, the depth at which the lobe shape deviated measurably from the equilibrium shape at Transect 73 was about 10 m whereas, further north at Transect 79, there remained a substantial bulge in the profile as shallow as 7 m. By 2012, the bathymetry had evolved towards the equilibrium shape to the extent that all of the lobe profiles were of very similar shape and their deviation from equilibrium was measurable only for $h > 12\text{ m}$ (Fig. 9 bottom). Close scrutiny of all profiles shows that, within survey error of generally less than $\pm 0.1\text{ m}$, bed level changes are evident across the lobe to about $h = 20\text{ m}$ but are negligible for $h = 21\text{ m}$.

Fig. 10 shows typical lobe profile evolution from 1966 to 2007 and to 2012 at Transect 75, within the alongshore lobe extent. Lobe bed level (z_i) deflation is greatest at about $h = 10\text{ m}$ and decreases seaward. Because of this, the seabed slopes (S) do not all shift monotonically towards the equilibrium slope. As shown in Fig. 11 for Transect 73, at $h = 10\text{ m}$, S has increased progressively while at $h = 12\text{ m}$, S has decreased initially to 1977 and then increased progressively. At $h > 12\text{ m}$, S has decreased through time and would be expected to increase again towards the equilibrium slope in the future. The lowest values of S occur at the mid depths $h = 14-16\text{ m}$ throughout this period of surveys.

Fig. 12 shows the cumulative change 1966 to 2012 at Transect 73 in the seaward position $x(h_i)$ of selected depth (h_i) contours relative to their 1966 positions. With the exception of the cyclone bar influence

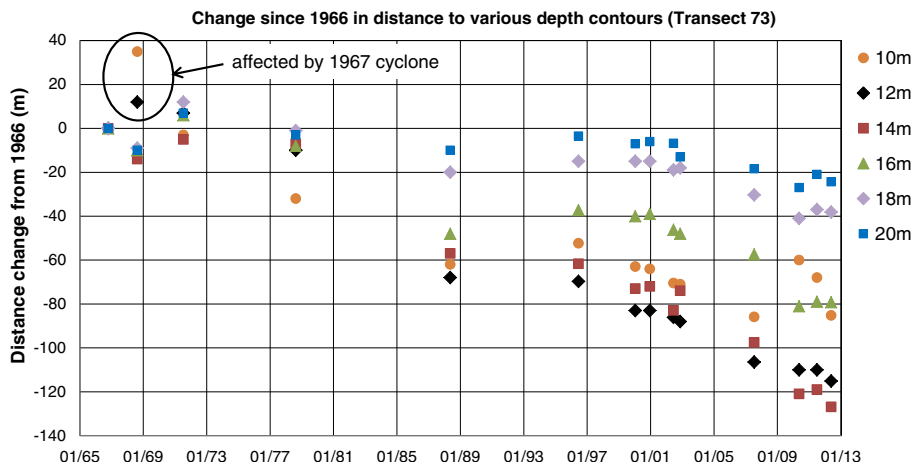


Fig. 12. Landward shift of various seabed depth contours at Transect 73 since 1966. Zero corresponds to the 1966 positions.

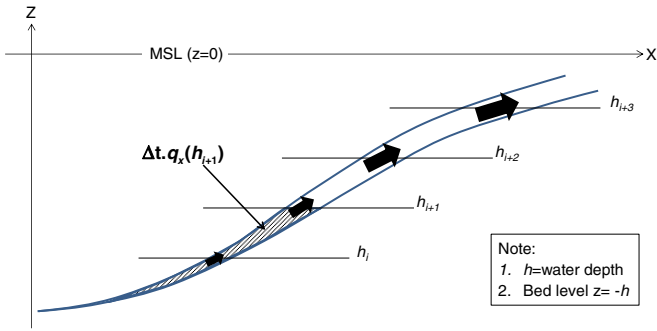


Fig. 13. Calculation of depth dependent q_x .

in 1967 for $h_i = 10\text{--}12\text{ m}$, all $x(h_i)$ chainages decrease progressively, indicating progressive lobe deflation. The greatest rate of shift in bed level contour chainage of 120 m over 46 years occurs at $12\text{ m} < h < 14\text{ m}$, corresponding to the zone of lowest and reducing S , compared to 20 m at $h = 20\text{ m}$. Consistency of the decreasing chainages during lobe deflation indicates reasonable survey accuracy.

5. Disequilibrium sand transport during lobe depletion

5.1. Framework

Changes in lobe seabed levels (z_s) may result from sediment transport gradients as per:

$$\frac{dz_s}{dt} = - \left(\frac{dq_x}{dx} + \frac{dq_y}{dy} \right) \tag{1}$$

where x extends across-shore and y is alongshore.

The lobe is located well seaward of the surf zone beyond the influence of wave radiation stress forcing (Fig. 7). Nevertheless, a non-zero long term net q_y may result from alongshore components of q in the direction of travel of waves approaching oblique to the coast. This would be directed northward due to the predominant east-southeast sector wave directions (Fig. 2). Importantly, there is alongshore uniformity of the lobe bathymetry such that it has little or no gradient where the greatest lobe depletion occurs, north from Transect 72 (Fig. 6). It can therefore be assumed reasonably that dq_x/dx is the dominant factor

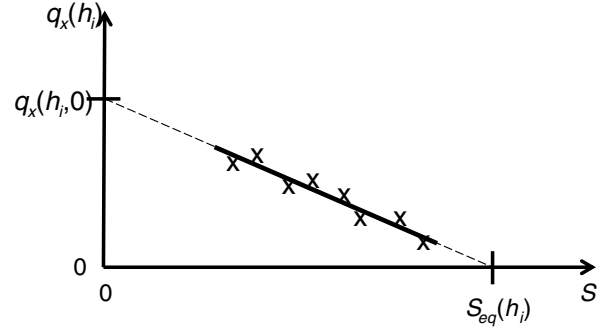
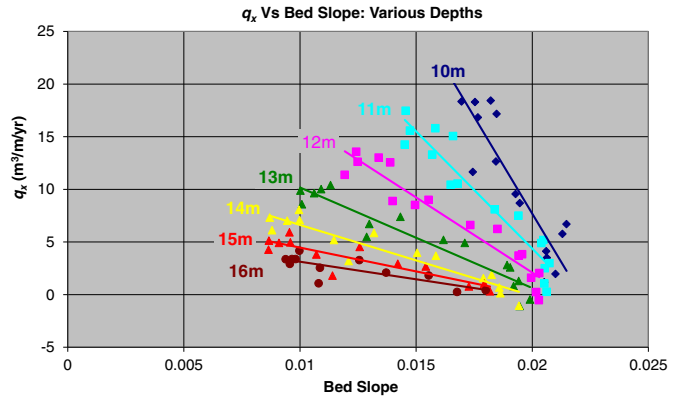


Fig. 15. q_x versus S measured (top); conceptual linear trend intercepts (bottom).

causing lobe depletion, due to shoreward q_x along the shoreface lobe extent, and that dq_y/dy is negligible even though q_y may not be. Additional support for this is that:

- There has been no measured gain of sand and significantly less lobe depletion at its southern extremity where its alongshore bathymetry gradient is maximum;
- There is no measurable sand gain at the toe of the shoreface; and
- Andrews and Nielsen (2001) showed that alongshore sand transport past the sand bypassing system to the river bar occurs within the littoral zone, with most probably a slight southward leakage of sand from the bar to the lobe in deeper water.

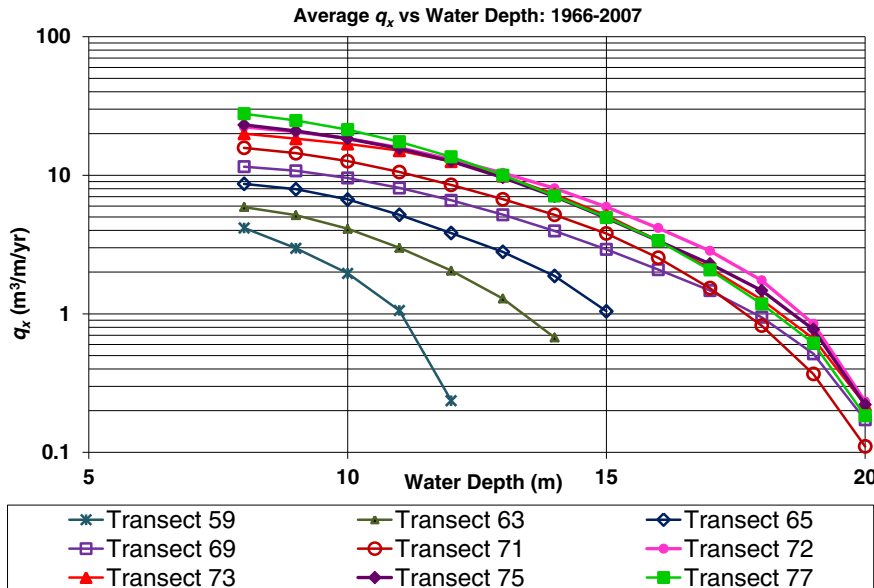


Fig. 14. Shoreward sand transport derived from the 1966 and 2007 surveys.

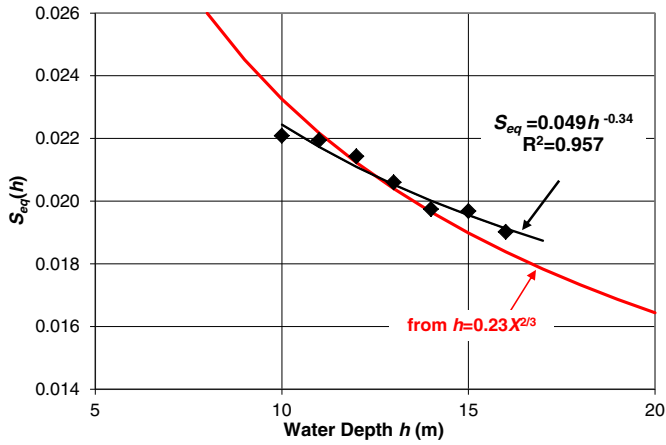


Fig. 16. Equilibrium bed slopes derived from data in Fig. 13.

Thus, the framework for the analysis of q_x is based on lobe depletion being due to gradients in shoreward transport of the sand dq_x/dx . Conceptually, the sand moves shoreward into the littoral zone where it is then subject to wave induced alongshore transport. It is recognized that correlation of theoretical methods (e.g. van Rijn et al., 2004) with the q_x rates derived from the data must make the provision $q_x = q_x \cos \theta$ where θ is the angle of wave travel to shore-normal. Our calculations as described in the last section of this paper show that this has only about 2.7% effect on the 5 year average q_x rate for this site over the period 2007–2012.

5.2. q_x rates 1966–2007

Analysis of the lobe profile changes has been undertaken in terms of the shoreward integral of volume change across specified depths, rather than distances, as illustrated in Fig. 13. Rates of q_x have been analysed initially for the 1966–2007 period of comprehensive data from the changes in profile volume per unit longshore length below each specified depth (h) as:

$$q_x(h) = q_x(h_0) + \int_{h_0}^h \frac{\partial x(h)}{\partial t} dh \quad (\text{bulk m}^3/\text{m}/\text{year}) \quad (2)$$

with $h_0 = -21$ m where it is assumed $q_x = \text{zero}$.

The $q_x(h)$ values thus derived represent long term average rates $\bar{q}_x(h)$ that have resulted from the forcing of the wave conditions incident over the period between the two dates of survey analysed, given from time t_0 to t_1 as:

$$\bar{q}_x(h) = \frac{1}{(t_1 - t_0)} \int_{t_0}^{t_1} q_x(h, t) dt \quad (3)$$

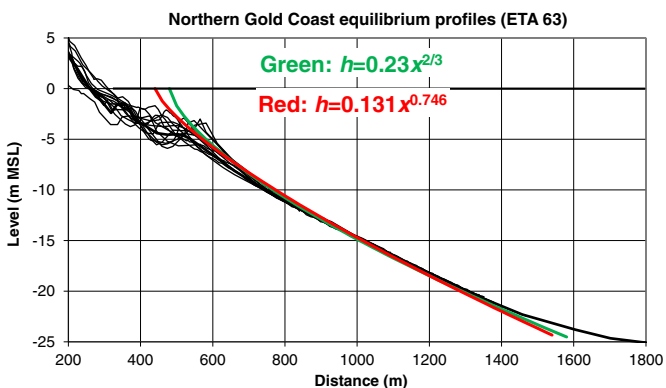


Fig. 17. Comparison of equilibrium profile shapes relative to the ETA 63 profiles.

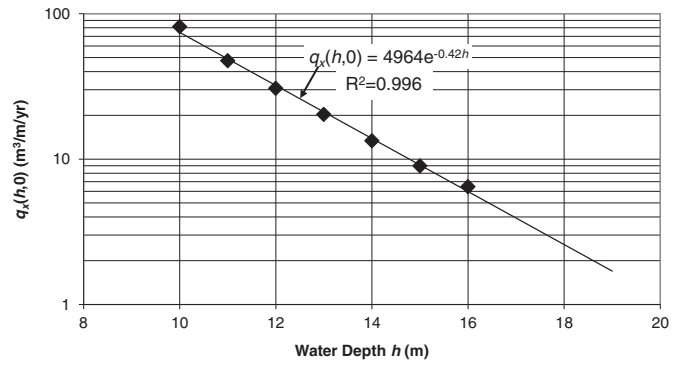


Fig. 18. Potential horizontal bed transport rates $q_x(h,0)$ derived from Fig. 15.

The assumption $q_x = 0$ at $h = 21$ m is not strictly valid if there is a persistent net supply of sand from the inner continental shelf to the shoreface. However, it is probable that this would have reduced over the 6000 year Holocene still-stand period to a sufficiently small rate at that depth such that errors in the calculated rates of transport at shallower depths are relatively minor.

The average q_x rates derived from the 1966 and 2007 surveys are shown in Fig. 14. These show depth dependence at each profile and significant differences between the transects along the lobe. The maximum average q_x rates range up to about 15–20 $\text{m}^3/\text{m}/\text{yr}$ at 10 m depth north from Line 72, and reduce progressively towards about 0.2–0.3 $\text{m}^3/\text{m}/\text{yr}$ at 20 m. They reduce markedly at the southern end of the lobe south from Line 69 towards the area where the profiles are closer to equilibrium. The measured q_x rate at Line 59 is only about 2.0 $\text{m}^3/\text{m}/\text{yr}$ at 10 m and diminishes markedly further seaward. Patterson (2007a,b) showed that this shoreward supply of sand explained the shoreline stability along this section of coastline despite a marked positive gradient in the longshore transport rate there.

The q_x rates derived represent the wave conditions during the survey period 1966–2007. Wave data is not available for that entire period, having commenced recording at a nearby Gold Coast location in 1986. The available dataset indicates a long term median significant wave height (H_s) of 1.05 m, spectral peak periods (T_p) typically of 7–12 s and irregular occurrences of storm and cyclone events with $H_s > 5$ m. Different q_x rates would be expected for periods with different wave conditions, influenced predominantly by occurrences of large cyclone waves.

The variation along and across the lobe indicates that q_x depends also on bed slope (S) or rather, on the deviation from the equilibrium slope. This slope dependence has been explored on the basis of the measured transport rates at common depths for each of the varying profiles along the lobe. These are presented as a series of $q_x(h_i)$ versus bed slope relationships for various water depths h_i in Fig. 15 (top). This indicates an approximately linear relationship between q_x and S at each depth and a variation in the relationship with water depth.

5.3. Depth and slope dependence of $q_x = q_x(h, S)$

These data suggest a series of linear relationships for each depth. To the extent that linear trend lines may be extrapolated to both axes (Fig. 15 bottom), their q_x intercept corresponds to horizontal bed transport rates $q_x(h, 0)$ (zero bed slope) and their S intercept corresponds to ‘equilibrium’ bed slopes (S_{eq}).

That is, these linear relations have the form:

$$q_x(h, S) = q_x(h, 0) \left[1 - \frac{S}{S_{eq}(h)} \right] \quad (4)$$

The term in brackets represents the slope dependent term providing for bed slope such that the actual average net shoreward sand transport

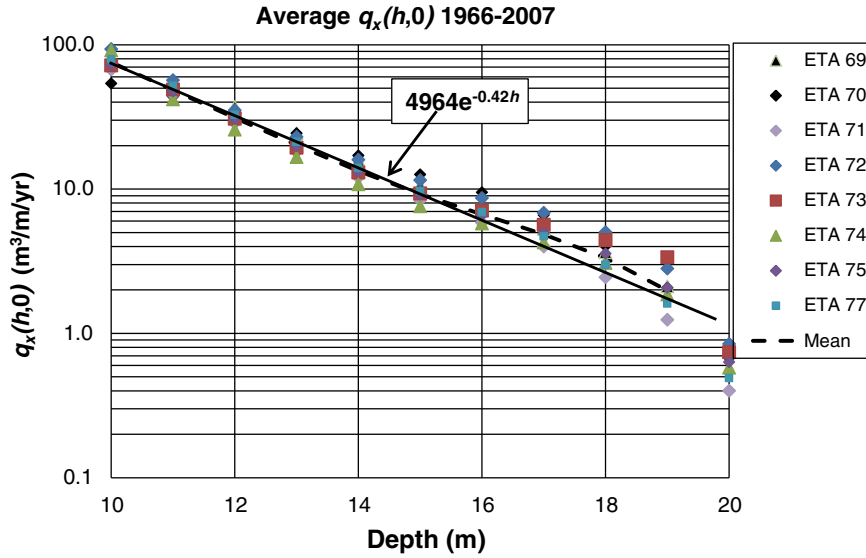


Fig. 19. $q_x(h,0)$ rates derived from Eq. (9).

(q_x) at any time is proportional to both a depth dependent potential (horizontal bed) annual average transport $q_x(h,0)$ and the difference between the actual and equilibrium bed slopes at any depth.

The S_{eq} estimates are shown as a function of depth in Fig. 16. The best power law fit to the data with goodness of fit $R^2 = 0.957$ is given by:

$$S_{eq}(h) = 0.049h^{-0.34} \quad (5)$$

Also shown in Fig. 16 (in red) are the equilibrium slopes derived from $h = Ax^{2/3}$ for $A = 0.23 \text{ m}^{1/3}$.

$$S_{eq}(h) = \frac{dh}{dx} = \frac{2}{3}A^{1.5}h^{-0.5} \quad (6)$$

While the match is reasonable within the accuracy of the data and methodology, the shape of the measured data best fit given by Eq. (5) does not match that for the Dean profile in which $S_{eq} \propto h^{-0.5}$. In fact, Eq. (5) corresponds to:

$$h = 0.131x^{0.746} \quad (7)$$

The two $S_{eq}(h)$ relationships are compared in Fig. 17 relative to data from Transect 63. They are empirically not too different at the water depths considered in this analysis. Similarly, the equivalent horizontal bed transport rates $q_x(h,0)$ have been extracted from the trend lines in

Fig. 15 at $S = 0$. The resultant $q_x(h,0)$ values are shown in Fig. 18. The best fit exponential fit with $R^2 = 0.996$ is:

$$q_x(h,0) = 4964e^{-0.42h} \quad (\text{bulk volume } \text{m}^3/\text{m}/\text{yr}) \quad (8)$$

The measured depth-dependent bed slopes and $q_x(h,S)$ may be used in conjunction with the adopted $S_{eq}(h)$ values to calculate the equivalent horizontal bed transport rates using the bed slope factor, in the form:

$$q_x(h,0) = q_x(h,S) \left(1 - \frac{S}{S_{eq}(h)} \right) \quad (9)$$

The $q_x(h,0)$ values are a function only of depth and the wave conditions and should not vary along the lobe. That is, Eq. (9) may be used to assess the reliability of the method in terms of the scatter of $q_x(h,0)$ values for all of the profiles along the lobe. These are calculated using Eq. (5) for $S_{eq}(h)$, as illustrated in Fig. 19, together with Eq. (8).

The spread of results relative to the average value for each depth is acceptably small to indicate validity of the method. However, at depths 17–19 m the values lie generally above the trend line, indicating either measurement inaccuracy or that S_{eq} given by Eq. (5) is an underestimate in this range. At 20 m depth the $q_x(h,0)$ values are significantly below trend, indicating that the assumption of $q_x = 0$ at 21 m is incorrect and that there is a shoreward sand supply of about $0.5 \text{ m}^3/\text{m}/\text{yr}$ from

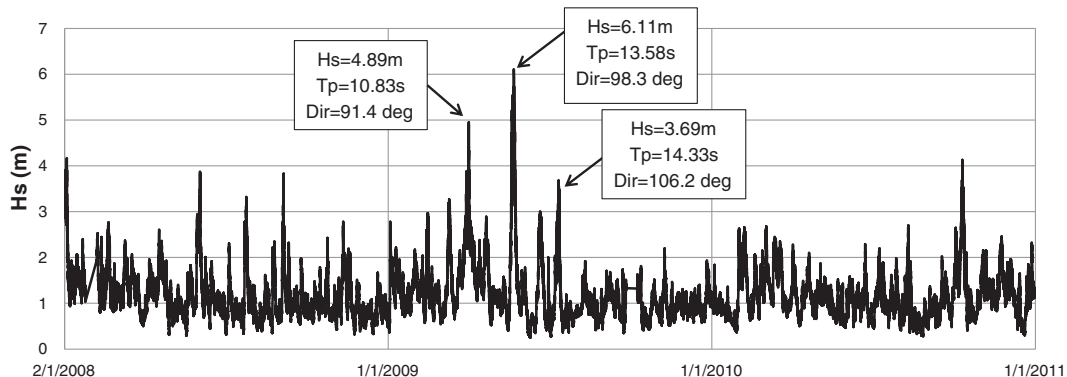


Fig. 20. Recorded significant wave heights (H_s) 2008–2010.

Table 1
Duration of exceedance of storm wave heights $H_s > 4-6$ m.

Year	Duration exceedance (hours)		
	$H_s > 4$ m	$H_s > 5$ m	$H_s > 6$ m
2003	-	-	-
2004	14.0	10.0	-
2005	1.5	-	-
2006	29.5	0.5	-
2007	12.0	-	-
2008	1.5	-	-
2009	86.7	30.3	0.5
2010	1.0	-	-
2011	3.0	-	-
2012	32.0	5.0	0.5

the inner shelf to the shoreface. This is however an insignificant correction to the q_x values at shallower depths.

6. Measured Gold Coast lobe q_x and derived $q_x(h,0)$ rates to 2012

Recent lobe profile survey data now available for this research to 2012 is of particular value, having been measured using more accurate

and comprehensive methods than were available in 1966, particularly with the advent of wave heave compensators, automated satellite positioning and digital data processing. As well, wave recording against which sand transport rates may be correlated commenced in 1986 and included directions from 2007.

It is evident from the wave data that storm wave conditions vary considerably from year to year. A particularly prolonged period of high waves of relatively long period occurred in the early part of 2009 (Fig. 20). The unusual nature of the high wave conditions in 2009 is indicated in Table 1 in terms of the annual durations of exceedance of storm waves of $H_s = 4-6$ m for the 10 years from 2003 to 2012 (inclusive) and in Fig. 21 showing the annual exceedance durations of $H_s = 4$ m over 1987–2012, with reference to the longer term average of 15.5 h.

Furthermore, wave periods associated with the highest waves range up to about 14 s, with high Ursell number (HL^2/d^3) for which wave asymmetry and shoreward sand transport would be expected to be relatively strong.

The lobe profile changes have been analysed for the average q_x for the extended survey period 1966–2012 and also for the most recent 5 year period 2007–2012 using the same procedures as outlined above (Fig. 22). The former extends the previous analysis to 46 years

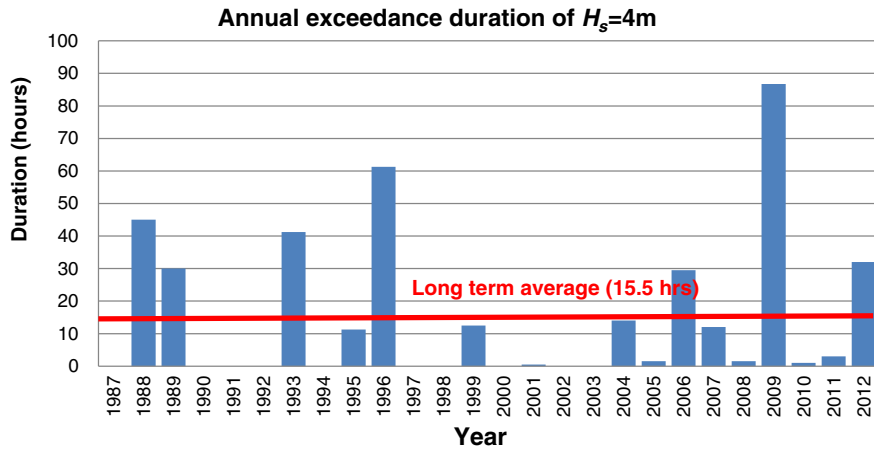


Fig. 21. Annual exceedance durations of $H_s = 4$ m 1987–2012.

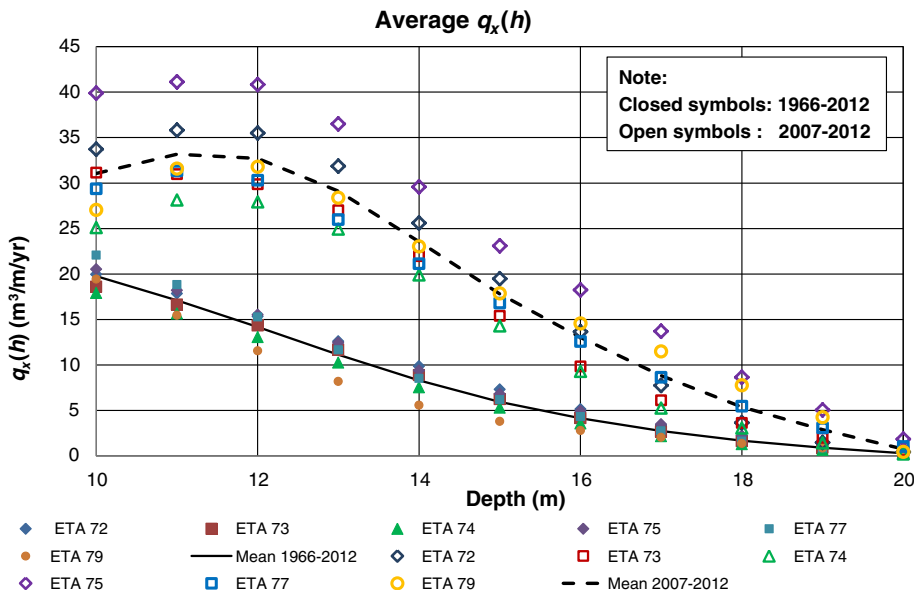


Fig. 22. Measured q_x rates 1966–2012 (closed symbols) & 2007–2012 (open symbols).

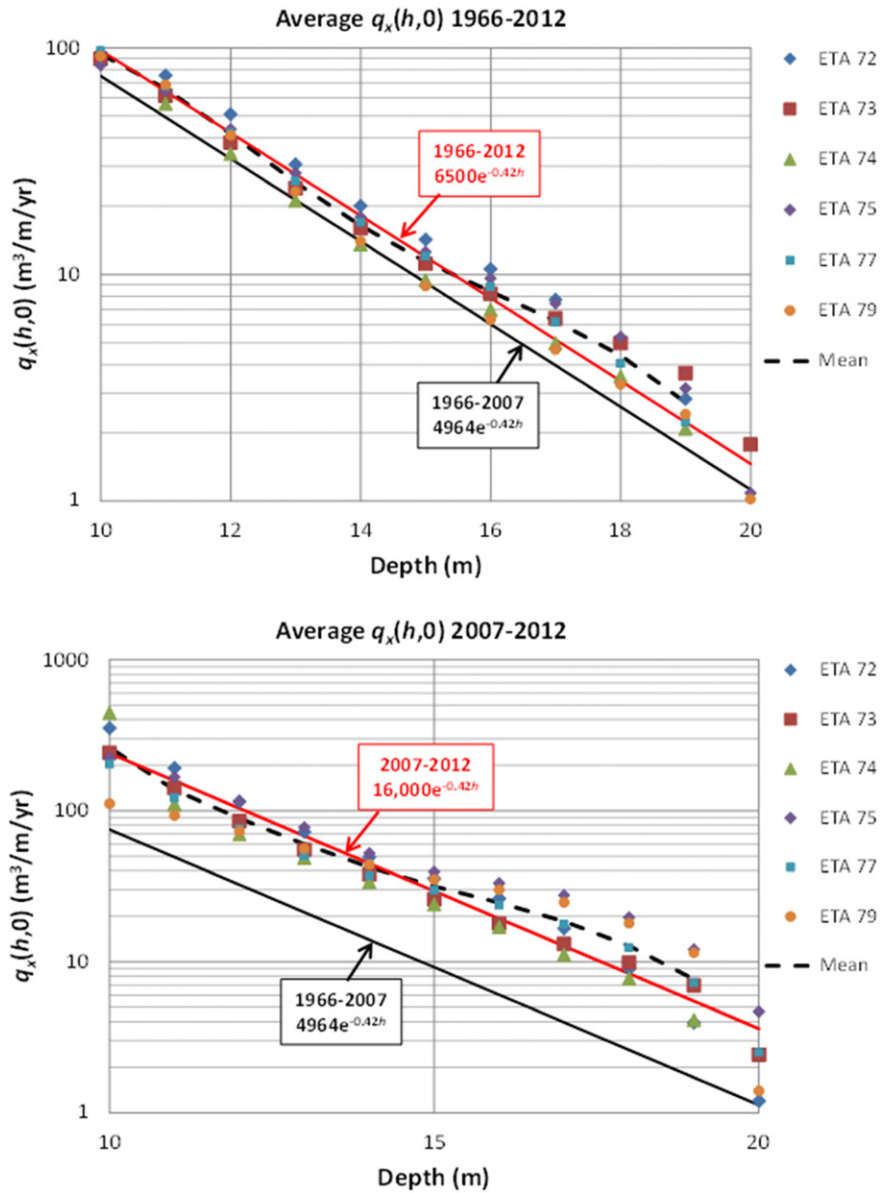


Fig. 23. Measured $q_x(h,0)$ rates 1966–2012 (top) & 2007–2012 (bottom).

to better represent the long term average conditions. The latter period emphasizes the behavior during that limited period, in particular the effects of the large storm event in 2009.

Similarly, the $q_x(h,0)$ rates have been analysed using Eq. (9) and $S_{eq}(h)$ given by Eq. (5) for the periods 1966–2012 and 2007–2012, as shown in Fig. 23. The $q_x(h,0)$ rates are compared directly in Fig. 24.

The extended long term analysis from 1966 to 2012 shows similar average annual q_x and $q_x(h,0)$ rates to those obtained for the period to 2007, though about 30% higher. The equivalent results for the shorter period 2007–2012 show significantly higher q_x rates and $q_x(h,0)$ rates over 3 times those for 1966–2007, indicating a direct response to the storm events in 2009. This establishes that $q_x(h,0)$ is dependent on both water depth and wave conditions. It remains to be specified how $S_{eq}(h)$ across the lower shoreface depends on the prevailing waves.

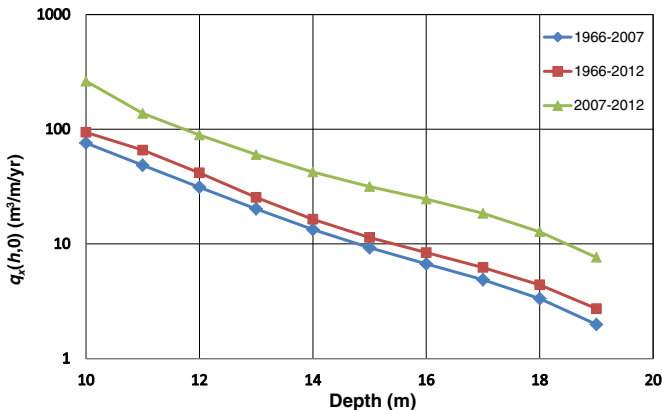


Fig. 24. Comparison of $q_x(h,0)$ rates 1966–2007; 1966–2012; 2007–2012.

7. Discussion

7.1. Depth, slope wave dependence of q_x

A database of long term surveys documenting progressive evolution of disequilibrium lobe profiles at depths of 10–20 m has been analysed to provide average rates of shoreward sand transport (q_x) under the wave conditions prevailing at the northern Gold Coast. The analysis

Table 2
Comparison of $q_x(h,0)$ by van Rijn et al. (2004) method with measured data at various depths for the period 2007 to 2012.

	Shoreward transport $q_x(h,0)$ for water depths shown ($\text{m}^3/\text{m}/\text{yr}$)		
	12 m	15 m	18 m
Measured data	89.1	31.6	12.8
Van Rijn et al	97.5	56.8	34.6

identifies a generally applicable form of relationship for q_x (Eq. (4)) that is the product of:

- a horizontal bed transport potential $q_x(h,0)$ that is dependent on both wave conditions and water depth; and
- the bed slope disequilibrium factor $[1 - \frac{S}{S_{eq}}]$.

These factors have been quantified for this particular location in terms of both long term (41–46 years) shoreface response and a shorter recent five year period during which there was an unusually high occurrence of storm waves of $H_s > 4\text{--}6$ m compared with the long term average. The lobe response during the period of relatively high waves shows that q_x increases with increased wave energy through the depth-dependent forcing component $q_x(h,0)$.

The analysis shows that the shoreface equilibrium profile has a best fit value $A \approx 0.23$ ($\text{m}^{1/3}$) for the shape of form $h = Ax^n$ with $n = 2/3$. However, it indicates the possibility that $n \approx 0.746$ for which the equivalent $A = 0.131$ ($\text{m}^{0.235}$). Observed $q_x(h,0)$ decrease with increasing water depth approximately as $q_x(h,0) = Ce^{-0.42h}$ where, with q_x is expressed as bulk $\text{m}^3/\text{m}/\text{year}$, C varies with wave conditions prevailing during the period considered. $C \approx 5000$ $\text{m}^3/\text{m}/\text{year}$ for the long term average 1966–2007. However, C is higher at 6,500 $\text{m}^3/\text{m}/\text{year}$ for the extended period 1966–2012 and ≈ 16000 $\text{m}^3/\text{m}/\text{year}$ for the 5 years 2007–2012 due to the unusually severe wave conditions in 2009.

While the average transport rates and bed slope factor derived through this analysis may be applied to determine shoreface response behavior over mid (years) to long (decades-centuries) timescales at this location, a method for analysis of transport under specified wave conditions is required for shorter timescales and for application to other locations. For this, theoretical methods may be applied, requiring calibration and/or validation against our measured rates.

7.2. Application of findings to theoretical methods and other locations

The significance of the findings of this research is that they provide a basis for testing the validity of theoretical methods and other models developed by various researchers. In that regard, all of the necessary data are available from the respective authorities in terms of profile surveys, sediment characteristics and recorded waves and water levels. While direct correlation of instantaneous sand transport rates and wave conditions is difficult in field conditions, the averaged rates between surveys may be calculated from theory using Eq. (3) and compared with the measured data for the same period.

Commonly, the theoretical methods seek to calculate q_x rates for a horizontal bed and then, as appropriate, apply a slope dependent factor (e.g. van Rijn et al., 2004). Our results confirm that the prototype conditions may be expressed in those terms and provide the opportunity to assess each component either separately or in combination. Van Rijn et al. (2004) determines bed load and suspended load separately, providing for wave asymmetry, boundary layer streaming and the net seaward flow below the wave trough, as well as other superimposed currents. Near-bed wave orbital currents are determined using empirical parameterized component relationships, from which bed load is calculated incrementally through the wave period in terms of instantaneous shear stresses. A period-averaged shear stress is used to

determine a representative near-bed suspended sediment concentration (C_a) from which suspended load is calculated.

The method of van Rijn et al. (2004), modified to remove shallow water theory assumptions in the deeper water involved, has been used to calculate average $\bar{q}_x(h,0)$ rates given by Eq. (3) for the study site using the recorded wave time series data for 2007–2012 for 12 m, 15 m and 18 m depths. Wave direction is accounted for using $q_x = q\cos\theta$ at each incremental wave recording in the time series, where θ is the wave angle to shore-normal. The results in bulk $\text{m}^3/\text{m}/\text{yr}$ assuming a solids volume of 65% are compared with the measured data in Table 2.

These results indicate encouraging agreement overall, with close correlation at 12 m but increasing over-prediction at greater depth. We found that providing for incident wave angle had about 2.7% effect in reducing $\bar{q}_x(h,0)$ relative to $\bar{q}(h,0)$ for this site.

Masetti et al. (2008) adopted a relationship of the form $q_x = K(h)[S_{eq}(h)-S]$ in which they assumed the depth-dependent forcing coefficient $K(h)$ reduces linearly with depth. This is equivalent to our Eq. (4) with $K(h) = q_x(h,0)/S_{eq}$ from which it is evident that the linear assumption for K is not appropriate and is more closely approximated as exponential.

Clearly, the specific transport rates measured for the Gold Coast are unique to that site because of their demonstrated dependence on wave conditions, in addition to any sediment influences. Nevertheless, we propose the equations derived here are of generally applicable form. Further, theoretical methods that are applied in generic models may be validated by correlation with the measured data at this location. In particular, the relative differences between the longer term average transport rates and those for the shorter period with unusually high waves provide an ideal basis on which wave climate differences may be determined or validated.

Acknowledgments

The analyses are based on or contain data provided by the City of Gold Coast, Queensland and the State of Queensland both of which give no warranty in relation to the data (including accuracy, reliability, completeness or suitability) and accept no liability (including without limitation, liability in negligence) for any loss, damage or costs (including consequential damage) relating to any use of the data. We acknowledge and thank the Queensland Department of Environment and Resource Management and the Gold Coast City Council for access to the wave and survey data used in this research.

References

- Andrews, M., Nielsen, C., 2001. Numerical modelling of the Gold Coast Seaway. Proc. 15th Australasian Coastal and Ocean Engineering Conf., Gold Coast, September, pp. 469–473.
- Bailard, J.A., 1981. An energetics total load sediment transport model for plane sloping beach. J. Geophys. Res. 86 (C11).
- Bruun, P., 1954. Coast Stability Doctoral dissertation Technical University of Denmark.
- Bruun, P., 1962. Sea level rise as a cause of shoreline erosion. J. Waterw. Harb. Div. Am. Soc. Civ. Eng. 88, 117–130.
- Bruun, P., 1986. The Bruun rule of erosion by sea-level rise: a discussion on large scale two and three-dimensional usages. J. Coast. Res. 4 (4), 527–648 Charlotteville.
- Dean, R.G., 1977. Equilibrium beach profiles: US Atlantic and Gulf Coasts. Ocean Engineering Report No.12. Dept Civil Engineering, University of Delaware, Newark, DE.
- Dean, R.G., 1991. Equilibrium beach profiles—characteristics and applications. J. Coast. Res. 7 (1), 53–84.
- Hallermeier, R.J., 1977. Calculating a yearly limit depth to beach erosion. Proc. 16th Coastal Engineering Conf., Hamburg, Germany, pp. 1493–1512.
- Hallermeier, R.J., 1981. A profile zonation for seasonal sand beaches from wave climate. Coast. Eng. 4 (3), 253–277.
- Inman, D.L., Elwany, M.H.S., Jenkins, S.A., 1993. Shorerise and bar-berm profiles on ocean beaches. J. Geophys. Res. 98 (C10).
- Larson, M., Kraus, N.C., Wise, R.A., 1999. Equilibrium beach profiles under breaking and non-breaking waves. Coast. Eng. 36, 59–85.
- Masetti, R., Fagherazzi, S., Montanari, A., 2008. Application of a barrier island translation model to the millennial-scale evolution of Sand Key, Florida. Cont. Shelf Res. 28, 1116–1126.

- Nielsen, P., 1992. Coastal bottom boundary layers and sediment transport. *Advanced Series on Coastal Engineering* vol. 4. World Scientific Publishing Co. Pte. Ltd.
- Nielsen, P., 2006. Sheet flow sediment transport under waves with acceleration skewness and boundary layer streaming. *Coast. Eng.* 53 (9), 749–758.
- Nielsen, P., Callaghan, D.P., 2003. Shear stress and sediment transport calculations for sheet flow under waves. *Coast. Eng.* 47 (3), 347–354.
- Patterson, D.C., 1999. Longshore transport modelling for Tweed River Entrance Sand Bypassing Project. *Coasts & Ports '99, Proc. 14th Australasian Coastal and Ocean Engineering Conference and the 17th Australasian Port and Harbour Conference*, Perth, April.
- Patterson, D.C., 2007a. Sand transport and shoreline evolution, Northern Gold Coast, Australia. *J. Coast. Res. Spec. Issue* 50.
- Patterson, D.C., 2007b. Comparison of recorded Brisbane and Byron wave climates and implications for calculation of longshore sand transport in the region. *Coasts and Ports 2007, Proc. 18th Australasian Conference on Coastal and Ocean Engineering*, Melbourne, July.
- Patterson, D.C., 2013. Modelling as an Aid to Understand the Evolution of Australia's Central East Coast in Response to Late Pleistocene–Holocene and Future Sea Level Change. PhD thesis, University of Queensland.
- Van Rijn, L.C., Walstra, D.J.R., van Ormondt, M., 2004. Description of TRANSPOR2004 and implementation in Delft3D-ONLINE. Report Z3748.10 for DG Rijkswaterstaat, Delft Hydraulics.